1521-009X/51/5/572–582$35.00
DRUG METABOLISM AND DISPOSITION
dx.doi.org/10.1124/dmd.122.001116
Drug Metab Dispos 51:572–582, May 2023

Preclinical Metabolism and Disposition of TP0473292, a Novel Oral Prodrug of the Potent Metabotropic Glutamate 2/3 Receptor Antagonist TP0178894 for the Treatment of Depression[S]

Shoko Inatani, Motoki Ochi, Kohnosuke Kinoshita, Jun-ichi Yamaguchi, and Hiromi Endo

Drug Metabolism and Pharmacokinetics, Drug Safety and Pharmacokinetics Laboratories, Research Headquarters, Taisho Pharmaceutical Co., Ltd., Saitama, Japan

Received September 16, 2022; accepted January 23, 2023

ABSTRACT

TP0473292 is an adamantane carboxylic acid (ACA) ester prodrug for enhancing the oral bioavailability of the hydrophilic glutamate analog TP0178894, a novel metabotropic glutamate 2 and 3 receptor antagonist, and being developed as an antidepressant. TP0473292 showed high membrane permeability and rapid hydrolysis to TP0178894 in rat, monkey, and human liver S9 fractions, with a conversion rate of such that complete conversion by first-pass metabolism was expected. TP0473292 was also hydrolyzed in the intestinal, renal, and lung S9 fractions, coinciding with the result that TP0473292 was activated by carboxylesterase (CES) 1 and more efficiently by CES2. Despite the rapid hydrolysis of TP0473292 in the intestinal S9 fraction, TP0473292 achieved good oral bioavailability of poorly permeable TP0178894 (approximately 60%) in rats and monkeys, with no TP0473292 detected in the plasma, revealing that rapid hydrolysis in the intestine is not necessarily a disadvantage. We also confirmed the penetration of TP0178894 into the cerebrospinal fluid and its unmetabolized excretion in urine. The ester promoiety, ACA, was metabolized to chemically stable acyl glucuronide and excreted in urine in rats and monkeys, suggesting a low risk of idiosyncratic drug toxicity. TP0473292 and its metabolites did not show a drug-drug interaction potential via cytochrome P450 in humans. These results suggested that TP0473292 functions as an ideal oral prodrug in humans; this was later confirmed to be true in phase 1 clinical trials. Furthermore, ACA was firstly confirmed to be a useful promoiety for hydrophilic drugs to enhance their oral bioavailability.

SIGNIFICANCE STATEMENT

Hydrolysis in the intestine reportedly has negative effects on the oral bioavailability of hydrophilic active metabolites of ester prodrugs. This study reports the preclinical pharmacokinetics of a hydrophilic metabotropic glutamate 2/3 receptor antagonist, TP0178894, and its ester prodrug TP0473292, which was found to act as an oral prodrug despite being activated predominantly in the intestine. Furthermore, this study firstly reports that adamantane carboxylic acid is useful as the ester promoiety of a prodrug for increasing lipophilicity and oral bioavailability.

Introduction

Abnormalities of glutamatergic transmission have been implicated in the pathophysiology of depression, and the group II metabotropic glutamate (mGlu) 2 and 3 receptors have potential as targets for the treatment (Chaki, 2017). The mGlu2/3 receptor antagonists reportedly have rapid and sustained antidepressant-like effects in rodent models, similar to (*R*,*S*)-ketamine (Chaki, 2017; Witkin, 2020), whose stereoisomer esketamine is used as an adjunct therapy for treatment-resistant depression, with the similar neural mechanisms to (*R*,*S*)-ketamine (Chaki and Fukumoto, 2019) but not showing (*R*,*S*)-ketamine associated side-effects (Witkin, 2020). These findings suggest that mGlu2/3 receptor antagonists hold promise as future antidepressants.

We previously discovered potent and selective mGlu2/3 receptor antagonists MGS0039 (BCI-632; Fig. 1A) and (1*R*,2*R*,3*R*,5*R*,6*R*)-2-amino-6-fluoro-3-[(4-fluorophenyl)methoxy]bicyclo[3.1.0]hexane-2,6-dicarboxylic acid (TP0178894) (Fig. 1B) (Nakazato et al., 2004). These were hydrophilic glutamate analogs, which possibly led to a low membrane permeability and, thus, a low oral bioavailability, making it difficult to develop them directly as oral antidepressants. In fact, MGS0039 showed a low oral bioavailability in rats (10.9%) and monkeys (12.6%) (Nakamura et al., 2006). Therefore, we adopted a prodrug strategy to increase its lipophilicity and synthesized MGS0210 (BCI-838; Fig. 1A), an *n*-heptyl alkyl ester prodrug of MGS0039. MGS0210 showed a relatively high conversion rate to MGS0039 in monkey and human liver S9 fractions among several ester prodrugs that were evaluated and an improved oral bioavailability (38.6%) as MGS0039 in monkeys (Nakamura et al., 2006). However, although MGS0210 was certainly absorbed, it mainly circulated in the plasma as the unchanged form, with approximately 10-fold higher exposure than MGS0039 in humans (Gadient et al., 2012), making it difficult to describe as an ideal prodrug

This work received no external funding.
All authors are employees of Taisho Pharmaceutical Co., Ltd.
dx.doi.org/10.1124/dmd.122.001116.
[S] This article has supplemental material available at dmd.aspetjournals.org.

ABBREVIATIONS: ACA, adamantane-1-carboxylic acid; ACA-AG, 1-*O*-(tricyclo[3.3.1.1^{3,7}]decane-1-carbonyl)-β-D-glucopyranuronic acid (adamantane-1-carboxylic acid acyl glucuronide); AUC, area under the concentration-time curve; BNPP, bis(p-nitrophenyl) phosphate; CES, carboxylesterase; CSF, cerebrospinal fluid; DDI, drug-drug interaction; EDTA-2K, EDTA dipotassium salt; F_{ads}, adsorption ratio; IDT, idiosyncratic drug toxicity; K_m, kinetic constant; K_{si}, substrate inhibition constant; LC-MS/MS, liquid chromatography–tandem mass spectrometry; $MgCl_2$, magnesium chloride; mGlu, metabotropic glutamate; PAMPA, parallel artificial membrane permeability assay; PMSF, phenylmethanesulfonyl fluoride; P450, cytochrome P450; [*S*], substrate concentration; SD, Sprague-Dawley; TP0178894, (1*R*, 2*R*, 3*R*, 5*R*, 6*R*)-2-amino-6-fluoro-3-[(4-fluorophenyl)methoxy]bicyclo[3.1.0]hexane-2, 6-dicarboxylic acid; TP0473292, (1*R*, 2*R*, 3*R*, 5*R*, 6*R*)-2-({(1*S*)-1-[(adamantane-1-carbonyl)oxy]ethoxy}carbonyl)-2-amino-6-fluoro-3-[(4-fluorophenyl)methoxy]bicyclo[3.1.0]hexane-6-carboxylic acid; $t_{1/2}$, half-life.

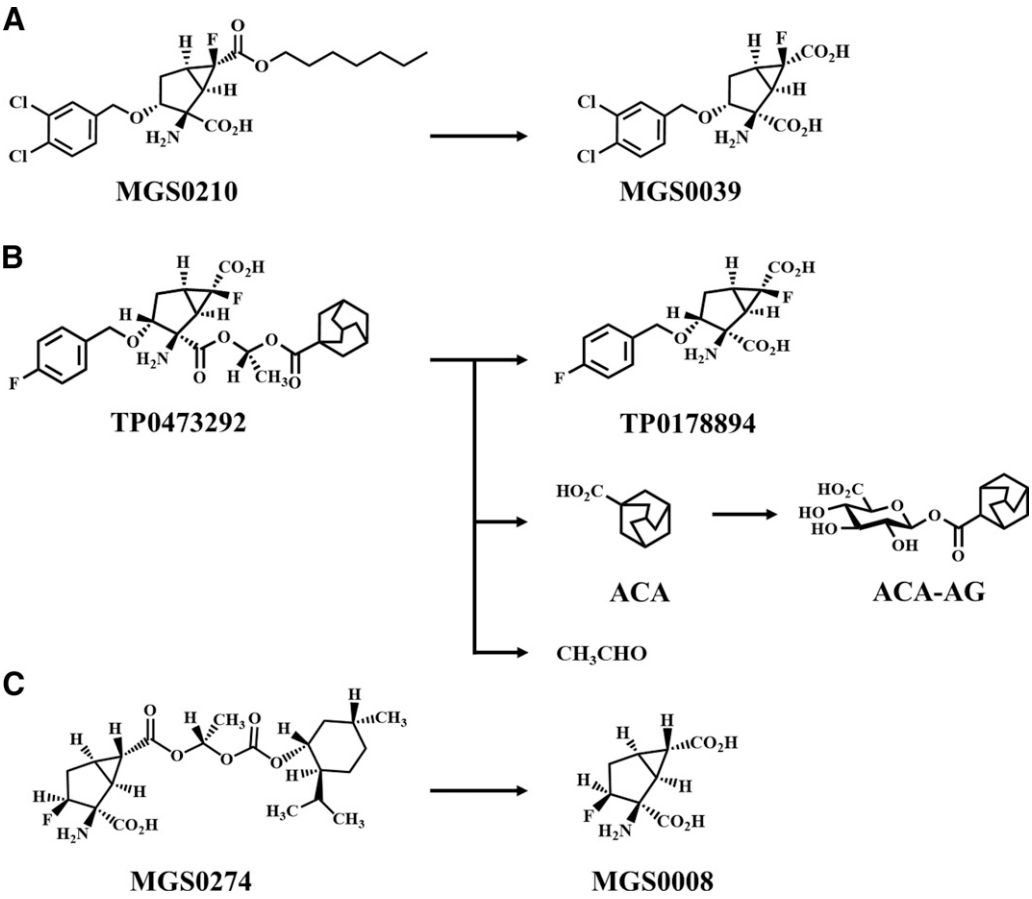

Fig. 1. Structures of ester prodrugs of glutamate analogs. (A) MGS0210: *n*-heptyl alkyl ester prodrug of an mGlu2/3 receptor antagonist MGS0039. (B) TP0473292: an adamantane carboxylic acid ester prodrug of an mGlu2/3 receptor antagonist TP0178894, shown with its proposed metabolic pathways in rat, monkey, and human cryopreserved hepatocytes. (C) MGS0274: an *l*-menthol ester prodrug of an mGlu2/3 receptor agonist MGS0008.

in terms of pharmacokinetics (Beaumont et al., 2003). A possible reason for the limited exposure to MGS0039 was that the conversion rate of MGS0210 to MGS0039 was not fast enough to achieve rapid and complete conversion. These results indicated that a successful oral prodrug would need to be converted much faster than MGS0210.

Subsequently, we confirmed this assumption by succeeding in the creation of MGS0274 besylate (Urabe et al., 2020; Fig. 1C), an *l*-menthol ester prodrug of an mGlu2/3 receptor agonist MGS0008 which was a glutamate analog and structurally similar to MGS0039 and TP0178894. MGS0274 exhibited a preferable lipophilicity and a higher conversion rate to its active metabolite than MGS0210 in monkey and human liver S9 fractions and achieved a high oral bioavailability (83.7%) as MGS0008 in monkeys with very low plasma exposure to MGS0274 (Kinoshita et al., 2019). In phase 1 clinical studies, MGS0274 was rapidly absorbed and extensively converted to MGS0008, whereas the plasma exposure to MGS0274 was low, approximately 3% of MGS0008 in a molar concentration, after oral administrations of MGS0274 besylate (Watanabe et al., 2020). Based on these results, we hypothesized that a prodrug with a high membrane permeability and faster conversion rate than MGS0274 would succeed as an ideal oral prodrug, even better than MGS0274.

Following this prodrug strategy, we synthesized a series of ester prodrugs of TP0178894 using various promoieties such as alkyl alcohols or *l*-menthol and selected (1*R*,2*R*,3*R*,5*R*,6*R*)-2-({(1*S*)-1-[(adamantane-1-carbonyl)oxy]ethoxy}carbonyl)-2-amino-6-fluoro-3-[(4-fluorophenyl)methoxy]bicyclo[3.1.0]hexane-6-carboxylic acid (TP0473292) (Fig. 1B) as the best. TP0473292 is a prodrug in which one of the carboxylic acids of TP0178894 is masked by adamantane-1-carboxylic acid (ACA) with two ester bonds to increase the lipophilicity. Adamantane is a promising moiety in drug design for providing lipophilicity to hydrophilic pharmacophores (Wanka et al., 2013). To apply an oral prodrug, adamantane should be conjugated with an active compound through a linker that is not chemically degradable, as in the case of a pH-sensitive linker in adamantane-conjugated doxorubicin prodrugs (González-Méndez et al., 2019), but is rapidly cleaved to release the active compound after absorption. Additionally, adamantane moiety should be cleared from the body without showing biologic activity, unlike amantadine prodrugs (Aboul-Fadl et al., 2011). Therefore, we used ACA as an inactive promoiety to conjugate adamantane with TP0178894 through two ester bonds, expecting not only increasing lipophilicity but also rapid enzymatic degradation. To our knowledge, there was no clinical prodrug that improves oral bioavailability of its active metabolite by adding adamantane through ester conjugation with ACA. Moreover, there was no report on the biologic fate of ACA as a liberated promoiety.

In this research, preclinical pharmacokinetic studies were conducted to evaluate whether TP0473292 could act as an ideal oral prodrug in humans. We also investigated the pharmacokinetic drug-drug interaction (DDI) potential of TP0473292 and its metabolites via cytochrome P450 (P450) in humans. Additionally, we firstly evaluated the usefulness of ACA as an ester promoiety for improving oral bioavailability of a hydrophilic compound.

Materials and Methods

Materials

TP0473292, TP0178894, and 1-*O*-(tricyclo[3.3.1.1^{3,7}]decane-1-carbonyl)-β-D-glucopyranuronic acid (adamantane-1-carboxylic acid acyl glucuronide) (ACA-AG) were synthesized at Taisho Pharmaceutical Co., Ltd. (Saitama, Japan). TP0473292 was synthesized by the method disclosed in the patent application (Otake et al., 2017). TP0178894 was synthesized by the previously reported method (Nakazato et al., 2004). ACA-AG was synthesized in reference to the reported method (Monrad et al., 2014). ACA was purchased from Tokyo Chemical

Industry Co., Ltd. (Tokyo, Japan). TP0181164, the structural analog of TP0178894, and the stable isotope-labeled TP0473292, TP0178894, ACA, and ACA-AG used as internal standards were also synthesized at Taisho Pharmaceutical Co., Ltd. in similar methods as to TP0178894 and each unlabeled compound described above. [^{3}H]TP0473292 was synthesized at Sekisui Medical Co., Ltd. (Tokyo, Japan). Benzil and bis(p-nitrophenyl) phosphate (BNPP) were purchased from Tokyo Chemical Industry Co., Ltd. Ethephon and EDTA dipotassium salt (EDTA-2K) dehydrate were purchased from FUJIFILM Wako Pure Chemical Corporation (Osaka, Japan). Phenylmethanesulfonyl fluoride (PMSF) was purchased from Merck KGaA (Darmstadt, Germany). Male Sprague-Dawley (SD) rat plasma (anticoagulant: EDTA-2K) and serum were obtained from HAMRI CO., LTD. (Ibaraki, Japan) and The Jackson Laboratory Japan, Inc. (Kanagawa, Japan), respectively. Cynomolgus monkey plasma (anticoagulant: EDTA-2K) and serum were purchased from HAMRI CO., LTD. Human plasma (anticoagulant: EDTA-2K) and serum were obtained from healthy male and female volunteers after review and approval by the Ethics Committee of Taisho Pharmaceutical Co., Ltd. The rat, monkey, and human plasma and sera were stored frozen at −80°C until use. Rat and monkey cryopreserved hepatocytes and human liver microsomes were purchased from Sekisui Xenotech, LLC (Kansas City, KS), and human cryopreserved hepatocytes were obtained from BioIVT (Westbury, NY). Cryopreserved primary human hepatocytes from three donors (two males and one female) were purchased from Thermo Fisher Scientific (Waltham, MA). Rat, monkey, and human tissue S9 fractions of the intestine (PMSF free), liver, lung, and kidney were obtained from Sekisui XenoTech, LLC. Recombinant human carboxylesterase (CES) 1 and CES2 bactosomes were purchased from Cypex Ltd. (Dundee, UK). All other reagents were of analytical grade or of high-performance liquid chromatography grade and were obtained from commercial sources.

Animals

Male SD rats (7 weeks old at the time of administration) were purchased from The Jackson Laboratory Japan, Inc. and were housed under controlled conditions with an approximate temperature (23°C ± 3°C), an approximate humidity (50% ± 20%), and lightning 12 hours/d at Taisho Pharmaceutical Co., Ltd. Male cynomolgus monkeys (8 years old at the time of administration; Simian Conservation Breeding & Research Center, Inc., Makati, Philippines) were housed under controlled conditions with an approximate temperature (24°C ± 3°C), an approximate humidity (50% ± 20%), and lightning 12 hours/d at Taisho Pharmaceutical Co., Ltd. Food was provided to rats ad libitum and monkeys once daily, except during fasting periods. Water was provided ad libitum. All the animal experimental procedures were approved by the Institutional Animal Care and Use Committee of Taisho Pharmaceutical Co., Ltd. and were performed in accordance with the 2006 Science Council of Japan Guidelines for Proper Conduct of Animal Experiments.

Parallel Artificial Membrane Permeability Assay

The membrane permeability of TP0473292 and TP0178894 at pH 6.2 was evaluated using a parallel artificial membrane permeability assay (PAMPA) evolution instrument (Pion Inc., Billerica, MA) according to the previously published method (Ochi et al., 2022). The bioanalysis was conducted by liquid chromatography–tandem mass spectrometry (LC-MS/MS) (Supplemental Table 1A).

Plasma Protein Binding

The plasma protein binding of TP0473292 in monkeys and humans was evaluated using an ultracentrifugation method. TP0473292 DMSO solution was spiked with monkey or human plasma (1:199, v/v) at a final concentration of 0.1 or 1 μg/ml. After 5-minute incubation at 37°C, an aliquot of the plasma sample was obtained for determining the concentration before ultracentrifugation. The remaining plasma sample was then ultracentrifuged at 627,379*g* for 4 hours at 10°C. After ultracentrifugation, an aliquot of the plasma supernatant was extracted using acetonitrile/methanol (9:1, v/v) containing the stable isotope-labeled TP0473292. The aliquot of the plasma sample obtained before ultracentrifugation was prepared to have the same compositions as that of the plasma supernatant samples. For the adsorption evaluation, a blank plasma supernatant, which was obtained by the ultracentrifugation of a blank plasma sample at 633,588*g* for 4 hours at 20°C, was spiked with TP0473292 DMSO solution (1:199, v/v) at a final concentration of 0.1 or 1 μg/ml and incubated for 4 hours at 10°C in the ultracentrifugation tube. The adsorption sample was prepared to have the same compositions as that of the plasma supernatant samples. Each sample was centrifuged at 3974*g* for 10 minutes at 4°C, and the resultant supernatant was subjected to LC-MS/MS analysis (Supplemental Table 1A). The stability of TP0473292 during ultracentrifugation was investigated, and TP0473292 was confirmed to be stable (>94% remaining after 4 hours of incubation at 10°C). The adsorption ratio (F_{ads}) and the percent of plasma protein binding were calculated using the following equations:

$$F_{ads}\ (\%) = (1 - C_2/C_1) \times 100 \quad (1)$$

$$\text{Protein binding}\ (\%) = \left(1 - \frac{C_{sup}/(100 - F_{ads}) \times 100}{C_p}\right) \times 100 \quad (2)$$

where C_1 is the theoretical initial concentration of TP0473292 in the adsorption sample, C_2 is the concentration of TP0473292 in the adsorption sample, C_{sup} is the concentration of TP0473292 in the plasma supernatant sample, and C_p is the concentration of TP0473292 in the plasma sample before ultracentrifugation. The plasma protein binding of TP0178894 was evaluated using an equilibrium dialysis method with a 96-well equilibrium dialysis plate (HTDialysis LLC, Gales Ferry, CT) and a 12–14 kDa cutoff dialysis membrane. TP0178894 was dissolved in DMSO and spiked with rat, monkey, or human plasma (1:199, v/v) at final concentrations of 0.1 and 10 μg/ml (rat and monkey) or 0.1 and 1 μg/ml (human). Each plasma sample was placed in the donor compartment of a 96-well equilibrium dialysis plate, and sodium phosphate buffer (50 mM, pH 7.4) containing sodium chloride (70 mM) was placed in the reservoir compartment. After incubation for 6 hours at a rate of 100 rpm at 37°C in humidified air (5% CO_2), an aliquot from each side of each well was collected and mixed with acetonitrile/methanol (9:1, v/v) containing the stable isotope-labeled TP0178894. Each sample was centrifuged at 3974*g* for 10 minutes at 4°C, and the resultant supernatant was subjected to LC-MS/MS analysis (Supplemental Table 1A). The protein binding (%) was calculated using the Boudinot formula (Boudinot and Jusko, 1984). The unbound fraction (%) was calculated as 100 – protein binding (%).

Hydrolysis of TP0473292 to TP0178894 in Rat, Monkey, and Human Sera and Tissue S9 Fractions

Rat, monkey, or human serum was prewarmed at 37°C, and TP0473292 DMSO solution was added at a final concentration of 50 μM. The rat, monkey, or human intestine, liver, kidney, or lung S9 fraction (0.001–0.1 mg protein/ml) in 250 mM sodium potassium phosphate buffer (pH 7.4), containing 74 mM potassium chloride, 2.4 mM magnesium chloride ($MgCl_2$), 1.4 mM glucose-6-phosphate, and 0.15 mM β-nicotinamide-adenine dinucleotide phosphate oxidized form, was prewarmed at 37°C, and then TP0473292 DMSO solution was added at a final concentration of 10 μM. For the enzyme kinetic studies using the human intestinal or liver S9 fraction, the protein concentration of 0.005 or 0.25 mg/ml and the TP0473292 concentration ranges of 10–500 or 10–1000 μM were used, respectively. The final concentration of DMSO in each incubation mixture was 1% or 1.2% v/v. After incubation for the designated times (1–60 minutes) at 37°C, the reaction was terminated by adding two volumes of acetonitrile/methanol (9:1, v/v) containing the stable isotope-labeled TP0178894, and the resultant mixture was centrifuged at 3974*g* for 10 minutes at 4°C. An aliquot of the supernatant was subjected to LC-MS/MS analysis to determine the concentration of TP0178894 (Supplemental Table 1A). The initial rate of TP0178894 formation was calculated as follows:

$$\begin{aligned}&\text{Initial rate}\ (\text{nmol/min/mg protein})\\ &= \text{Concentration of TP0178894}\ (\text{nmol/ml})/\text{Incubation time}\ (\text{min})\\ &\quad /\text{Protein concentration}\ (\text{mg protein/ml})\end{aligned} \quad (3)$$

The kinetic parameters of TP0473292 hydrolysis to TP0178894 in the human intestinal and liver S9 fractions were calculated using Phoenix WinNonlin (version 6.2 or higher; Certara, Princeton, NJ) using the traditional Michaelis-Menten equation and the substrate inhibition model as described below (Tachibana et al., 2005), respectively.

$$V_0 = \frac{V_{max} \times [S]}{K_m + [S] + [S]^2/K_{si}} \quad (4)$$

where V_0 is the initial rate of TP0178894 formation (nmol/min per mg protein), K_m is the kinetic constant (μM), V_{max} is the maximum rate of TP0178894

TABLE 1

Inhibitory effects of esterase inhibitors on the hydrolysis of TP0473292 to TP0178894 in the human liver S9 fraction
Values are presented as the mean of triplicate determinations.

Inhibitor	Enzyme	Concentration[a] (mM)	Reference	Percent Inhibition
Benzil	CES	0.1	Wadkins et al., 2005	99.5
BNPP	AADAC, CES, CMBL	1	Watanabe et al., 2009	99.7
Ethephon	BChE	0.1	Haux et al., 2002	−1.5
EDTA	PON	4	Umehara et al., 2016	10.7
PMSF	AADAC, BChE, CES	1	Watanabe et al., 2009	99.5

AADAC, arylacetamide deacetylase; BChE, butyrylcholinesterase; CMBL, carboxymethylenebutenolidase; PON, paraoxonase.
[a]The final concentration of each esterase inhibitor in the reaction mixture was set to a concentration that would sufficiently inhibit the target enzymes based on the reference articles.

formation (nmol/min per mg protein), [*S*] is the substrate (TP0473292) concentration (μM), and K_{si} is the substrate inhibition constant (μM).

Reaction Phenotyping

Chemical Inhibition Study. The effects of the esterase inhibitors, benzil, BNPP, ethephon, EDTA, and PMSF on the hydrolysis of TP0473292 (50 μM) to TP0178894 in the human liver S9 fraction were evaluated. The human liver S9 fraction was preincubated with each esterase inhibitor for 30 minutes on ice before starting the reaction. The reactions were performed as described in the hydrolysis study for the tissue S9 fractions. The final concentration of the human liver S9 fraction in the reaction mixture was 0.25 mg protein/ml and that of the organic solvent was 1.4% v/v. The final concentration of each esterase inhibitor in the reaction mixture was set at a concentration that would sufficiently inhibit the target enzymes based on the previous reports (Table 1). The percent inhibition was calculated as follows:

$$\text{Percent inhibition} = 100 - C_{inhibited}/C_{control} \times 100 \quad (5)$$

where $C_{control}$ is the concentration of TP0178894 in the absence of the inhibitor, and $C_{inhibited}$ is the concentration of TP0178894 in the presence of the inhibitor.

Metabolic Study in Recombinant Human CES. The reaction mixture, consisting of 75 μg/ml of recombinant human CES1 or CES2 and 49 mM phosphate buffer (pH 7.4), was prewarmed at 37°C. The reaction was initiated by adding TP0473292 DMSO solution (2.0% v/v) at a final concentration of 50 μM. After incubation for the designated times (1–15 minutes), the reaction was terminated by adding two volumes of acetonitrile/methanol (9:1, v/v) containing the stable isotope-labeled TP0178894. The resultant mixture was centrifuged at 2150*g* for 10 minutes at 4°C, and an aliquot of the supernatant was subjected to LC-MS/MS analysis (Supplemental Table 1A). The initial rate of TP0473292 hydrolysis to TP0178894 was calculated as described in the hydrolysis study for the tissue S9 fractions.

Metabolite Profiling of TP0473292 in Rat, Monkey, and Human Hepatocytes. Rat, monkey, or human cryopreserved hepatocytes suspended in Leivovitz L-15 medium containing 2 mM L-glutamine (0.5 million cells/ml) were incubated at 37°C for 1 hour with [^{3}H]TP0473292 and/or TP0473292 at 5 μM (0.1 MBq/ml). The reaction was terminated by adding acetonitrile containing acetic acid (0.1% v/v), and the resultant mixture was centrifuged at 2607*g* for 10 minutes at 4°C. Aliquots of the supernatant were analyzed using a high-performance liquid chromatograph equipped with a radiochemical flow detector. Aliquots of the supernatant from unlabeled incubation samples and authentic standards were also analyzed using liquid chromatography-mass spectrometry under the same chromatographic conditions, and their chromatographic retention times and mass spectral data were compared (Supplemental Table 1B).

Chemical Stability of Acyl Glucuronide. To evaluate the chemical stability of acyl glucuronide, the degradation rate of acyl glucuronide in the phosphate buffer was evaluated by two incubations (Jinno et al., 2013). First, the test compound (ACA, diclofenac, or ibuprofen) was incubated at 100 μM with pooled human liver microsomes (1 mg protein/ml) in 50 mM phosphate buffer (pH 7.4) containing 4.9 mM $MgCl_2$, 30 μg/ml alamethicin, and 2 mM saccharic acid 1,4-lactone to allow for the formation of acyl glucuronide. Reactions were initiated by adding uridine diphosphate glucuronic acid (5 mM) after 5-minute preincubation at 37°C. After 60-minute incubation, the reactions were terminated by adding 10% v/v acetic acid in acetonitrile/distilled water (1:1, v/v), and the resultant samples were subjected to a second incubation. Second, the aliquots of the resultant samples were spiked into 49 volumes of 200 mM phosphate buffer (pH 7.4) containing 5 mM $MgCl_2$ and further incubated for 0, 0.25, 0.5, 1, 2, and 4 hours to assess the stability of acyl glucuronide in the phosphate buffer. The reactions were terminated by adding 10% v/v acetic acid in acetonitrile/distilled water (1:1, v/v), and the resultant mixtures were subjected to LC-MS/MS analysis after centrifugation (Supplemental Table 1C). The degradation rate constant (k) was determined from the peak responses of acyl glucuronide versus the time curve using linear regression of the semilogarithmic plot, and the half-life ($t_{1/2}$) was calculated as follows: $t_{1/2} = \ln(2)/k$.

DDI Potential

P450 Reversible Inhibition. The inhibition potentials of TP0473292, TP0178894, ACA, and ACA-AG on the specific activities of seven human P450 isoforms were evaluated using enzyme specific substrates, phenacetin (CYP1A2), bupropion (CYP2B6), amodiaquine (CYP2C8), diclofenac (CYP2C9), (*S*)-mephenytoin (CYP2C19), bufuralol (CYP2D6), and midazolam and testosterone (CYP3A), according to a previously published method (Kinoshita et al., 2019). Briefly, the test compound was spiked into pooled human liver microsomes (0.1 mg/ml) at final concentrations of 0.1, 1, or 10 μM and prewarmed. After incubation with a marker substrate of each P450 isoform at a concentration near its K_m value (Michaelis constant), the reaction was terminated by adding acetonitrile. The concentration of the specific metabolite of each marker substrate was determined using the previously published LC-MS/MS method (Kinoshita et al., 2019).

P450 Time-Dependent Inhibition. The time-dependent inhibition potentials of TP0473292, TP0178894, ACA, and ACA-AG on the specific activities of seven human P450 isoforms were investigated using the same probe substrates as those used in the reversible inhibition study as well as pooled human liver microsomes according to a previously published method (Takano et al., 2021). Briefly, human liver microsomes (0.5 mg protein/ml) were incubated with the test compound (10 μM) for 30 minutes at 37°C to allow for the generation of intermediates that may inhibit P450 isoforms. Then, the first incubation mixture was diluted 10-fold with the second incubation mixture containing each probe substrate at a final concentration near fivefold of its K_m value. The second incubation was conducted for the designated time at 37°C and was terminated by adding acetonitrile. The concentration of the specific metabolite of each marker substrate in the second incubation mixture was determined using the previously reported LC-MS/MS method (Kinoshita et al., 2019).

P450 Induction. The CYP1A2, CYP2B6, and CYP3A4 induction potentials of TP0473292 and TP0178894 (0.1, 1, and 10 μM) were evaluated using mRNA levels in the primary cultured cryopreserved human hepatocytes according to a previously published method (Takano et al., 2021), with some modifications. The mRNA expression levels of CYP1A2, CYP2B6, and CYP3A4 were measured using a fluorescent-labeled microbead assay using the QuantiGene Plex 2.0 Plex Set (customized product of panel no. 12117) and the QuantiGene Plex 2.0 Assay Kit. The CYP1A2, CYP2B6, and CYP3A4 mRNA levels were normalized against the endogenous control gene (β-glucuronidase).

Pharmacokinetics in Rats and Monkeys. The pharmacokinetics of TP0473292 and TP0178894 in fasted male SD rats ($n = 3$) and fasted male cynomolgus monkeys ($n = 3$) were investigated. For intravenous administration, TP0178894 was dissolved in saline and administered to rats and monkeys (1 mg/kg). TP0473292 was dissolved in 10% w/v 2-hydroxypropyl-β-cyclodextrin containing 2.5% w/v mannitol and administered to rats and monkeys (1 mg/kg, 0.613-mg equivalent of TP0178894/kg). Blood samples were collected from the tail vein of rats or the cephalic vein of monkeys into tubes containing the anticoagulant EDTA-2K (rats and monkeys) and the esterase inhibitor PMSF (rats only) at

predose (monkeys only) and 5, 15, and 30 minutes and 1, 2, 4, 8, and 24 hours postdose, and then plasma samples were obtained after centrifugation. Urine samples were collected over the intervals of 0–24 hours (rats) or 0–8 and 8–24 hours (monkeys) into bottles containing 20% v/v acetic acid on ice. For oral administration, TP0178894 was suspended in 0.5% w/v methylcellulose 400 and administered to monkeys (1 mg/kg). TP0473292 was suspended in 0.5% w/v methylcellulose 400 and administered to rats (1 mg/kg, 0.613-mg equivalent of TP0178894/kg) and monkeys (1.63 mg/kg, 1-mg equivalent of TP0178894/kg). Blood samples were collected from the tail vein of rats or the cephalic vein of monkeys into tubes containing EDTA-2K (rats and monkeys) and PMSF (rats only) at 30 minutes and 1, 2, 4, 8, and 24 hours postdose (rats) or at predose, 30 minutes, and 1, 2, 3, 4, 6, 8, and 24 hours postdose (monkeys). The plasma or urine samples were precipitated with acetonitrile/methanol (9:1, v/v) containing the stable isotope-labeled TP0178894 or a mixture of the stable isotope-labeled TP0473292, TP0178894, ACA, and ACA-AG. Following centrifugation at 3639*g* for 10 minutes at 4°C, the aliquots of the supernatant were analyzed by LC-MS/MS (Supplemental Table 1, A and D). To evaluate the extent of the cerebrospinal fluid (CSF) penetration of TP0178894 in rats, TP0473292 was suspended in 0.5% w/v methylcellulose 400 and administered orally to nonfasted SD rats at a dose of 1 mg/kg (0.613-mg equivalent of TP0178894/kg). Blood samples were collected from the posterior vena cava into tubes containing EDTA-2K and PMSF under isoflurane anesthesia at 1, 2, 3, 4, 8, or 24 hours postdose. Then, the animal was euthanized by exsanguination, and CSF was drawn from the spinal cord space. The plasma or CSF was precipitated with acetonitrile/methanol (9:1, v/v) containing TP0181164, a structural analog of TP0178894, as an internal standard and centrifuged. Aliquots of the supernatant were analyzed by LC-MS/MS (Supplemental Table 1A).

Pharmacokinetic Analysis. The concentration-time profiles of TP0473292, TP0178894, ACA, and ACA-AG in plasma were analyzed using a noncompartmental analysis (Phoenix WinNonlin version 6.2).

Results

PAMPA Permeability

The membrane permeability of TP0473292 and TP0178894 at pH 6.2 was evaluated using a PAMPA at 10 μM. The apparent permeability of TP0473292 was 36.6×10^{-6} cm/s, whereas the apparent permeability of TP0178894 was estimated to be less than 0.03×10^{-6} cm/s since the concentrations in the acceptor solutions were below the lower limit of quantification (0.006 μM).

Plasma Protein Binding

The unbound fractions of TP0473292 at 0.1 and 1 μg/ml ranged from 1.7% to 1.8% in monkeys and 1.1% in humans. The protein binding of TP0473292 in rat plasma was not evaluated, because of its rapid hydrolysis to TP0178894. The unbound fractions of TP0178894 in rat, monkey, and human plasma (0.1 and 10 μg/ml in rats and monkeys, 0.1 and 1 μg/ml in humans) ranged from 87.6% to 87.9%, 100.4% to 101.0%, and 92.6% to 94.9%, respectively. These data indicate that there are no apparent species differences or concentration dependencies in plasma protein binding for TP0473292 or TP0178894.

Hydrolysis of TP0473292 to TP0178894 in Rat, Monkey, and Human Sera and Tissue S9 Fractions

The formation rates of TP0178894 from TP0473292 in rat, monkey, and human sera (50 μM TP0473292) and tissue S9 fractions (10 μM TP0473292) are shown in Table 2. The formation rate of TP0178894 in serum was much faster in rats than that in monkeys and humans, with a TP0473292 elimination $t_{1/2}$ of less than 1 hour, assuming complete conversion to TP0178894. In rats, the formation rate of TP0178894 was highest in the intestinal S9 fraction, followed by the lung, liver, and kidney S9 fractions. In monkeys, the formation rate of TP0178894 was higher in the intestinal and kidney S9 fractions than in the liver and lung S9 fractions. In humans, the formation rate of TP0178894 was higher in the liver and intestinal S9 fractions than the kidney and lung S9 fractions. The enzyme kinetics for the hydrolysis of TP0473292 to TP0178894 in human intestinal and liver S9 fractions were evaluated. The formation rates of TP0178894 ranged from 4.25 to 19.6 nmol/min per mg protein in the human intestinal S9 fraction for TP0473292 concentration ranges of 10–500 μM and from 15.9 to 204 nmol/min per mg protein in the liver S9 fraction for TP0473292 concentration ranges of 10–1000 μM. The Eadie-Hofstee plots showed that the hydrolysis of TP0473292 to TP0178894 exhibited Michaelis-Menten kinetics in the human intestinal S9 fraction and substrate inhibition kinetics in the human liver S9 fraction (Supplemental Fig. 1). The K_m in the human intestinal S9 fraction was calculated to be 40.3 μM, and the V_{max} was 21.3 nmol/min per mg protein. The K_m and K_{si} in the human liver S9 fraction were calculated to be 583 μM and 141 μM, respectively, and the V_{max} was 927 nmol/min per mg protein. The K_m value in the human intestinal S9 fraction was comparable to its solubility in the fed-state simulated intestinal fluid (data not shown), the assumed highest concentration in the gut. The K_m and K_{si} in the human liver S9 fraction were sufficiently higher than the plasma concentration at an effective dose in rat models (approximately 2 μM as TP0178894) and probably in humans as well since no species difference in antagonist activity was observed between rats and humans (Watanabe et al., 2022). These results indicated that TP0473292 hydrolysis would not be saturated in either the intestine or the liver at an effective dose in humans.

Reaction Phenotyping

Chemical Inhibition Study. The esterases involved in the hydrolysis of TP0473292 to TP0178894 in the human liver S9 fraction were estimated by selective chemical inhibition studies with five esterase inhibitors: benzil, BNPP, ethephon, EDTA, and PMSF. The inhibitory effects of these esterase inhibitors are shown in Table 1. The paraoxonase inhibitor EDTA and the butyrylcholinesterase inhibitor ethephon showed minimal inhibition of the hydrolysis of TP0473292 to TP0178894, indicating that neither paraoxonase nor butyrylcholinesterase was likely to be involved in the hydrolysis of TP0473292. BNPP and PMSF inhibited the hydrolysis of TP0473292 to TP0178894 completely, suggesting that CES and/or arylacetamide deacetylase were involved in the hydrolysis of TP0473292. Benzil, which inhibits CES but not arylacetamide deacetylase (Shimizu et al., 2014), also inhibited the hydrolysis of TP0473292 completely,

TABLE 2

Formation rate of TP0178894 from TP0473292 in rat, monkey, and human sera (50 μM TP0473292) and tissue S9 fractions (10 μM TP0473292)
Values are presented as the mean (S.D.) of triplicate determinations.

	Formation Rate of TP0178894 (nmol/min per mg protein)				
	Serum	Intestine	Liver	Lung	Kidney
Rat	0.0138 (0.000306)	52.1 (1.07)	1.32 (0.104)	2.26 (0.111)	0.962 (0.0870)
Monkey	0.000846 (0.0000172)	36.6 (3.97)	15.1 (0.965)	5.46 (0.0770)	26.5 (0.933)
Human	0.000491 (0.0000236)	4.25 (0.101)	9.84 (0.823)	0.781 (0.0559)	0.822 (0.0269)

suggesting that CES, but not arylacetamide deacetylase, was responsible for the hydrolysis of TP0473292. As CES4 is less sensitive to PMSF inhibition (Fujiyama et al., 2009), among CES1, CES2, and CES4 expressed in human liver, CES1 and/or CES2 were likely to be responsible for the hydrolysis of TP0473292 to TP0178894 in the human liver S9 fraction.

Metabolic Study in Recombinant Human CES. The formation rates of TP0178894 from TP0473292 (50 μM) in recombinant human CES1 and CES2 were 7.4 and 19.8 nmol/min per mg protein, respectively. These results indicated that the hydrolysis of TP0473292 to TP0178894 is mediated by both CES1 and, more efficiently, CES2.

Metabolite Profiling of TP0473292 in Rat, Monkey, and Human Hepatocytes. The metabolite profiles of TP0473292 in rat, monkey, and human cryopreserved hepatocytes were evaluated. In all the species, the predominant peak was identified as TP0178894 based on the mass spectral data and chromatographic retention time, and no other metabolite peak was detected by the high-performance liquid chromatograph equipped with the radiochemical flow detector (Fig. 2). In addition to TP0178894, the mass chromatograms detected ACA and ACA-AG in all the species (Supplemental Table 2). The proposed metabolic pathways of TP0473292 in rats, monkeys, and humans are shown in Fig. 1B. TP0473292 underwent enzymatic hydrolysis to yield TP0178894 and ACA, and ACA was further metabolized via glucuronidation to form ACA-AG. The further metabolism of TP0178894 was not observed, and no human-specific metabolites were found.

Chemical Stability of Acyl Glucuronide. The chemical stability of ACA-AG was evaluated in phosphate buffer (pH 7.4). ACA-AG showed a much longer degradation $t_{1/2}$ (79.2 hours) compared with the acyl glucuronides of diclofenac (1.23 hours) and ibuprofen (4.92 hours), which are classified as "warning" in terms of their idiosyncratic drug toxicity (IDT) risk (Sawamura et al., 2010).

DDI Potential

P450 Inhibition. The inhibitory potentials of TP0473292, TP0178894, ACA, and ACA-AG on seven human P450 isoforms, CYP1A2, CYP2B6, CYP2C8, CYP2C9, CYP2C19, CYP2D6, and CYP3A, were investigated using human liver microsomes. All the compounds had no inhibitory potential for any of the P450 isoforms at concentrations up to 10 μM in a reversible or a time-dependent manner (Supplemental Table 3).

P450 Induction. The induction potentials of TP0473292 and TP0178894 on CYP1A2, CYP2B6, and CYP3A4 mRNA expressions were evaluated using three lots of primary cultured cryopreserved human hepatocytes at a concentration of 0.1, 1, or 10 μM. TP0473292 or TP0178894 did not produce marked changes in CYP1A2, CYP2B6, or CYP3A4 mRNA levels at concentrations up to 10 μM (Supplemental Table 4). Since ACA and ACA-AG were probably formed during the TP0473292 induction study, both metabolites were thought to have no apparent induction potential on the tested P450 mRNA.

Pharmacokinetics of TP0178894 in Rats and Monkeys. The plasma concentration-time profiles of TP0178894 after a single

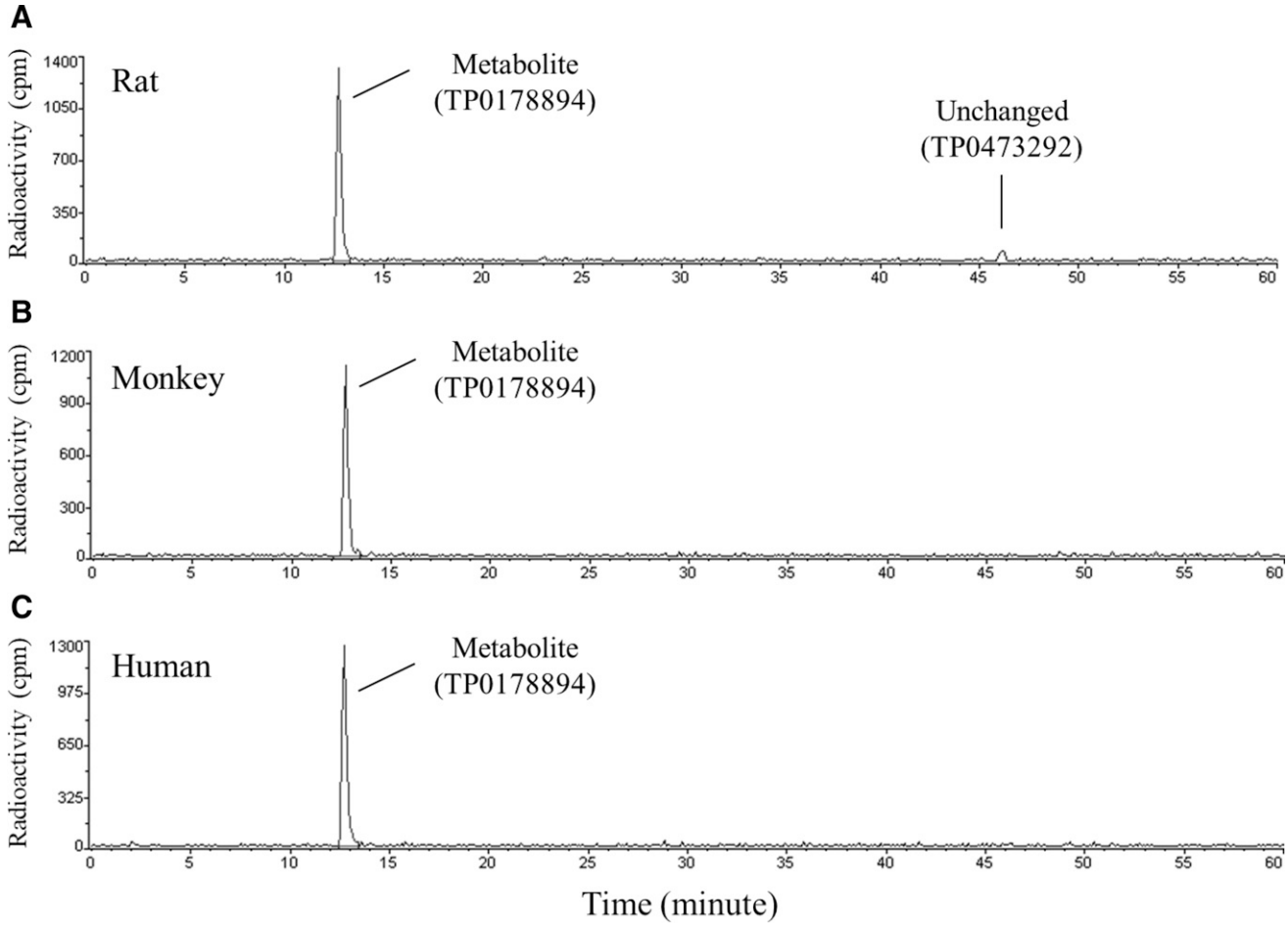

Fig. 2. HPLC radiochromatograms of the incubation mixtures of [^{3}H]TP0473292 with rat (A), monkey (B), and human (C) cryopreserved hepatocytes. [^{3}H]TP0473292 (5 μM) was incubated with rat, monkey, or human cryopreserved hepatocytes at 0.5 million cells/ml at 37°C for 1 hour.

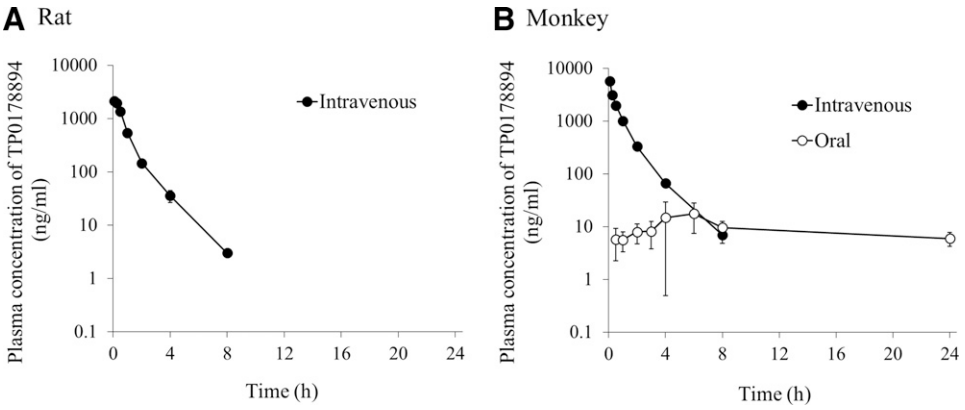

Fig. 3. Plasma concentration-time profiles of TP0178894 after a single intravenous or oral administration of TP0178894 to fasted male SD rats (A) or cynomolgus monkeys (B) at a dose of 1 mg/kg. Data are represented as the mean ± S.D. of three animals. The lower limit of quantification was 1 ng/ml for rats and 0.5 ng/ml for monkeys.

intravenous administration of TP0178894 (1 mg/kg) to male rats and monkeys and that after a single oral administration of TP0178894 (1 mg/kg) to male monkeys under fasted conditions are shown in Fig. 3. The pharmacokinetic parameters are summarized in Table 3. After the intravenous administration of TP0178894, the plasma TP0178894 level rapidly decreased, with an elimination $t_{1/2}$ of 1.08 hours in rats and 1.82 hours in monkeys. The volume of distribution at steady state was low: 473 ml/kg in rats and 258 ml/kg in monkeys. The excretion of TP0178894 into urine within 24 hours postdose was 76.6% of the dose in rats and 97.4% of the dose in monkeys. The renal clearance was calculated to be 403 ml/h per kg in rats and 263 ml/h per kg in monkeys. After the oral administration of TP0178894 to monkeys, TP0178894 slowly reached a plasma C_{max} of 22.6 ng/ml at 3.50 hours postdose and then slowly declined with a $t_{1/2}$ of 20.0 hours. The oral bioavailability was estimated to be 5.8%.

Pharmacokinetics of TP0473292 in Rats and Monkeys. The plasma concentration-time profiles of TP0473292, TP0178894, ACA, and ACA-AG after a single intravenous or oral administration of TP0473292 to male rats (1 mg/kg, 0.613-mg equivalent of TP0178894/kg) and monkeys (1 or 1.63 mg/kg, 0.613- or 1-mg equivalent of TP0178894/kg, respectively) under fasted conditions are shown in Fig. 4 and Fig. 5, respectively. The pharmacokinetic parameters are summarized in Table 4 and Table 5, respectively. After the intravenous administration of TP0473292 to rats and monkeys, TP0473292 rapidly declined with a $t_{1/2}$ of 0.375–0.624 hours. TP0178894 was detected from the first sampling time point (5 minutes postdose), reaching a C_{max} at 0.500–0.917 hours postdose, followed by a gradual decline ($t_{1/2}$ = 1.09–3.54 hours), compared with TP0473292. The plasma levels of ACA, liberated together with TP0178894 from TP0473292, and its acyl glucuronide, ACA-AG, immediately reached their C_{max} within 0.25 hours postdose and declined with a $t_{1/2}$ of less than 3 hours. The urinary excretion of TP0178894 and ACA-AG within 24 hours postdose was 80.3% and 65.6% of the administered dose in rats and 85.7% and 71.1% in monkeys, respectively. The excretion of TP0473292 and ACA into urine was less than 1.5% of the administered dose in both species. After the oral administration of TP0473292 to rats and monkeys, TP0178894 was detected from the first sampling time point (30 minutes postdose) and reached a C_{max} at 1.00–2.67 hours postdose. TP0178894 declined with a $t_{1/2}$ of 1.44–4.68 hours, which was slightly slower than that after intravenous administration. TP0473292 was not detected in plasma in both animals. The oral bioavailability of TP0178894 after TP0473292 administration was 58.4% in rats and 56.6% in monkeys, which was approximately 10-fold higher than that after the oral administration of TP0178894 itself in monkeys (5.8%). The plasma levels of ACA and ACA-AG immediately reached their C_{max} within 2 hours postdose and declined with a $t_{1/2}$ of approximately 4 to 5 hours, which was slower than that after intravenous administration. The extent of CSF penetration of TP0178894 after a single oral administration of TP0473292 was evaluated in nonfasted male rats at a dose of 1 mg/kg (Fig. 6; Table 6); at this dose, the immobility time in the rat forced-swimming test was previously reported to be significantly reduced (Watanabe et al., 2022). The CSF concentration of TP0178894 reached a C_{max} at 3 hours postdose, which was later than that in plasma (1 hour) and decreased at a slower rate than that in plasma. The area

TABLE 3

Pharmacokinetic parameters of TP0178894 after a single intravenous (fasted male SD rats and fasted male cynomolgus monkeys) or oral (fasted male cynomolgus monkeys) administration of TP0178894 at a dose of 1 mg/kg

Data are presented as the mean (S.D.) of three animals.

Species	Rat	Monkey	
Route	Intravenous	Intravenous	Oral
Dose	1 mg/kg	1 mg/kg	1 mg/kg
CL_{total} (ml/h per kg)	526 (17.0)	270 (12.5)	—
Vd_{ss} (ml/kg)	473 (28.7)	258 (32.0)	—
$t_{1/2}$ (h)	1.08 (0.0173)	1.82 (1.38)	20.0 (4.73)
C_{max} (ng/ml)	—	—	22.6 (11.4)
t_{max} (h)	—	—	3.50 (2.78)
AUC[a] (h·ng/ml)	1900 (60.0)	3710 (166)	213 (71.1)
F[b] (%)	—	—	5.8 (2.1)
UE[c] (% of dose)	76.6 (8.47)	97.4 (11.4)	NT

—, not applicable; CL_{total}, total plasma clearance; F, bioavailability; NT, not tested; t_{max}, time to reach maximum concentration; UE, urinary excretion; Vd_{ss}, volume of distribution at steady state.

[a] $AUC_{0-\infty}$ for the intravenous administration, AUC_{0-24} for the oral administration.

[b] F = (AUC_{0-24} following the oral administration)/($AUC_{0-\infty}$ following the intravenous administration) × 100.

[c] Urinary excretion within 24 hours postdose.

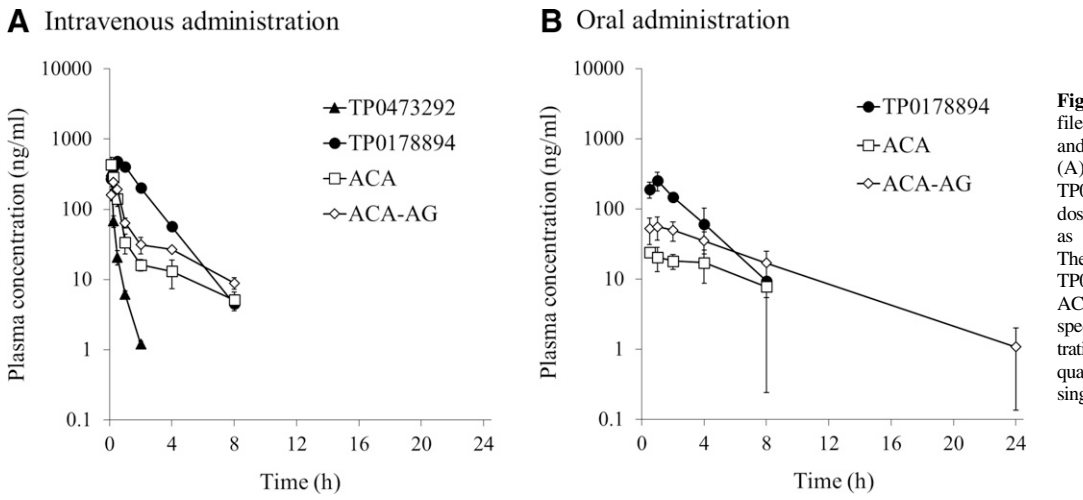

Fig. 4. Plasma concentration-time profiles of TP0473292, TP0178894, ACA, and ACA-AG after a single intravenous (A) or oral (B) administration of TP0473292 to fasted male SD rats at a dose of 1 mg/kg. Data are represented as the mean ± S.D. of three animals. The lower limits of quantification for TP0473292, TP0178894, ACA, and ACA-AG were 1, 1, 3, and 1 ng/ml, respectively. Plasma TP0473292 concentrations were below the lower limit of quantification at all time points after a single oral administration of TP0473292.

under the concentration-time curve (AUC) from 0 to 8 hours of CSF was 1.5% of that in plasma.

Discussion

We investigated the preclinical pharmacokinetics of an mGlu2/3 receptor antagonist TP0178894 and its ACA-conjugated ester prodrug TP0473292 to determine whether TP0473292 would be an ideal oral prodrug in humans.

TP0178894 showed low permeability in a PAMPA and a low oral bioavailability (5.8%) in monkeys. In rats and monkeys, the volume of distribution at steady-state values of TP0178894 were low despite being mostly free in the plasma. Almost all of the intravenously dosed TP0178894 was excreted unchanged in the urine, and its metabolism was not observed in the hepatocytes, indicating that renal excretion was a major elimination pathway in both species. These results probably originated from the hydrophilicity of TP0178894 (cLogP = 1.21), leading us to adopt a prodrug strategy.

TP0473292 (cLogP = 4.59), a lipophilic prodrug of TP0178894, was synthesized based on the strategy of creating a highly permeable prodrug with a higher conversion rate than our previous successful oral prodrug MGS0274 (Watanabe et al., 2020). TP0473292 showed increased permeability and high conversion rates to TP0178894 in rat, monkey, and human tissue S9 fractions, with a rate more than threefold higher (9.84 nmol/min per mg protein) than that of MGS0274 (3.14 nmol/min per mg protein) in the human liver S9 fraction (Kinoshita et al., 2019). The rapid hydrolysis of TP0473292 was also confirmed in vivo by intravenous administration of TP0473292 in the animals.

An ideal prodrug for improved oral bioavailability targeting the systemic exposure of its active metabolite reportedly needs to have good stability in gastrointestinal cells (Trapa et al., 2017). A CES1, not CES2, substrate is considered preferable as CES1 and CES2 are the major hydrolases in the liver and the intestine in humans, respectively (Di, 2019). However, TP0473292 was a substrate for both isoforms and was unstable in the intestinal S9 fractions from all the species tested, unlike the CES1 substrate MGS0274 (Ochi et al., 2022). These results raised concern regarding the low oral bioavailability of TP0473292 as hydrophilic TP0178894. However, TP0473292 achieved a good oral bioavailability of approximately 60% as TP0178894 in rats and monkeys, where the hydrolysis of TP0473292 in the intestinal S9 fractions was much faster than that in humans. Since TP0473292 was not detected in the plasma, TP0473292 seemed to have been completely hydrolyzed by first-pass metabolism in both species. TP0473292 had much higher K_m (583 μM) and V_{max} (927 nmol/min per mg protein) values in human liver S9 fractions than MGS0274 (Km: 17.5 μM; Vmax: 8.87 nmol/min per mg protein), *l*-menthol ester prodrug of MGS0008 (Ochi et al., 2022), suggesting that ACA promoiety contributed to achieve the high turnover rate and complete hydrolysis. We assumed that TP0473292 was converted to TP0178894 mostly in the enterocytes in monkeys because the intrinsic clearance of TP0178894 formation in the intestinal S9 fraction (3660 μl/min per mg protein) was higher than the reported value for the hydrolysis of mycophenolate mofetil (3059 μl/min per mg protein), which is an ester prodrug of mycophenolic acid and has a low intestinal

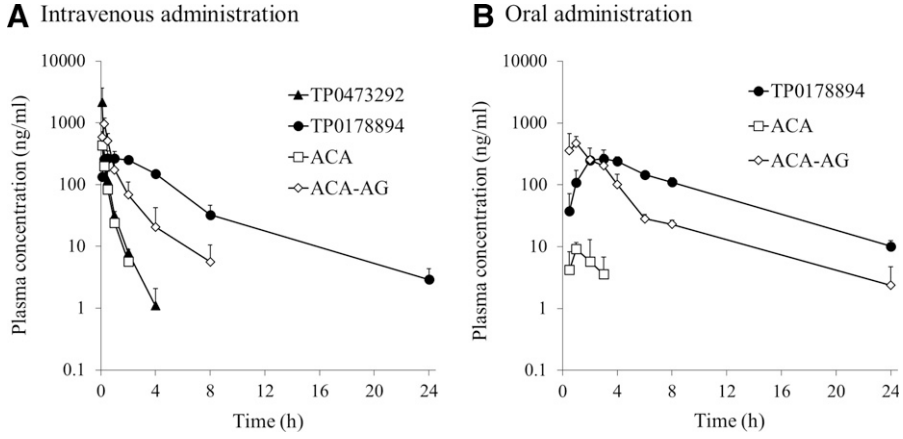

Fig. 5. Plasma concentration-time profiles of TP0473292, TP0178894, ACA, and ACA-AG after a single intravenous [(A) 1 mg/kg] or oral [(B) 1.63 mg/kg] administration of TP0473292 to fasted male cynomolgus monkeys. Data are represented as the mean ± S.D. of three animals. The lower limits of quantification for TP0473292, TP0178894, ACA, and ACA-AG were 1, 1, 3, and 1 ng/ml, respectively. Plasma TP0473292 concentrations were below the lower limit of quantification at all time points after a single oral administration of TP0473292.

TABLE 4

Pharmacokinetic parameters of TP0473292, TP0178894, ACA, and ACA-AG after a single intravenous or oral administration of TP0473292 to fasted male SD rats at 1 mg/kg

Data are presented as the mean (S.D.) of three animals.

Species	Rat							
Route	Intravenous				Oral			
Dose	1 mg/kg				1 mg/kg			
Analyte	TP0473292	TP0178894	ACA	ACA-AG	TP0473292[a]	TP0178894	ACA	ACA-AG
CL_{total} (ml/h per kg)	10,900 (1810)	—	—	—	—	—	—	—
Vd_{ss} (ml/kg)	2280 (590)	—	—	—	—	—	—	—
$t_{1/2}$ (h)	0.375 (0.0364)	1.09 (0.0351)	2.90 (0.472)	2.78 (0.469)	NC	1.44 (0.442)	3.74 (0.0208)	3.84 (1.03)
C_{max} (ng/ml)	—	484 (14.5)	437 (117)	243 (33.1)	NC	256 (76.2)	25.3 (3.67)	58.0 (17.8)
t_{max} (h)	—	0.500 (0.00)	0.0833 (0.00)	0.250 (0.00)	NC	1.00 (0.00)	1.83 (1.89)	2.00 (1.73)
$AUC_{0-\infty}$ (h·ng/ml)	93.9 (16.0)	1010 (27.0)	275 (61.3)	358 (21.4)	NC	681 (156)	161 (36.1)	372 (56.3)
F (%)	—	—	—	—	NC	58.4[b]	—	—
UE[c] (% of dose)	0.0[a] (0.0)	80.3 (4.11)	1.3 (0.35)	65.6 (3.10)	NT	NT	NT	NT

—, not applicable; CL_{total}, total plasma clearance; F, bioavailability; NC, not calculated; NT, not tested; t_{max}, time to reach maximum concentration; UE, urinary excretion; Vd_{ss}, volume of distribution at steady state.

[a]TP0473292 concentrations in plasma and urine samples were below the lower limit of quantification (1 ng/ml).

[b]Bioavailability was calculated by dividing the dose-normalized $AUC_{0-\infty}$ of TP0178894 following oral administration of TP0473292 by the dose-normalized $AUC_{0-\infty}$ of TP0178894 following intravenous administration of TP0178894 shown in Table 3.

[c]Urinary excretion within 24 hours postdose was calculated by dividing excreted amount of the analyte compound (μmol) by the dose of TP0473292 (μmol).

availability (Trapa et al., 2017). The possible reasons for the good bioavailability of hydrophilic TP0178894 despite the presumably rapid formation in the enterocytes were as follows: TP0178894 formed in the enterocytes might have permeated more extensively to the basolateral side than to the luminal side by passive diffusion, depending on a steep concentration gradient maintained by the blood flow or according to the pH-partitioning theory, as reported for acidic compounds (Masaki et al., 2006), and/or by active transport. Of these, we considered that active transport was less likely based on the following kinetic analysis. In monkeys, the elimination of TP0178894 in the plasma after the oral administration of TP0473292 was slower than that after the intravenous administration of TP0178894, which would reflect the slow "absorption" of TP0178894. This slow absorption would likely have originated from the slow permeation of TP0178894 from the enterocytes into the blood, but not the dissolution and permeation of TP0473292 from the gut lumen into the enterocytes, because ACA, which is liberated from TP0473292 simultaneously with TP0178894, showed a different, faster elimination. Assuming the "flip-flop" pharmacokinetics of TP0178894 after the oral administration of TP0473292 in monkeys, the absorption rate constant (k_a) of TP0178894 was estimated to be 0.15 1/h. Then, the effective permeability (P_{eff}) was roughly estimated to be 0.1×10^{-4} cm/s using the following equation:

$$k_a = \frac{2P_{eff}}{R} \quad (6)$$

where R refers to the monkey small intestine radius, 0.35–0.45 cm (Takahashi et al., 2010), which was lower than the reported value for low permeable atenolol in monkeys (0.37×10^{-4} cm/s) (Takahashi et al., 2010). Although a detailed kinetic analysis is needed, these results suggested that the TP0178894 absorption after the oral administration of TP0473292 can be sufficiently explained by the slow passive diffusion of TP0178894 originated from its hydrophilic structure and is not likely to

TABLE 5

Pharmacokinetic parameters of TP0473292, TP0178894, ACA, and ACA-AG after a single intravenous (1 mg/kg) or oral (1.63 mg/kg) administration of TP0473292 to fasted male cynomolgus monkeys

Data are presented as the mean (S.D.) of three animals.

Species	Monkey							
Route	Intravenous				Oral			
Dose	1 mg/kg				1.63 mg/kg			
Analyte	TP0473292	TP0178894	ACA	ACA-AG	TP0473292[a]	TP0178894	ACA	ACA-AG
CL_{total} (ml/h per kg)	2210 (1070)	—	—	—	—	—	—	—
Vd_{ss} (ml/kg)	559 (342)	—	—	—	—	—	—	—
$t_{1/2}$ (h)	0.624 (0.175)	3.54 (0.418)	0.389 (0.0600)	1.22 (0.312)	NC	4.68 (0.520)	NC	4.70 (2.73)
C_{max} (ng/ml)	—	299 (53.9)	430 (28.7)	964 (223)	NC	266 (46.0)	10.4 (3.86)	518 (106)
t_{max} (h)	—	0.917 (0.946)	0.0833 (0.00)	0.250 (0.00)	NC	2.67 (0.577)	1.33 (0.577)	1.17 (0.764)
$AUC_{0-\infty}$ (h·ng/ml)	570 (367)	1400 (145)	140 (15.3)	727 (140)	NC	2100 (230)	NC	1320 (322)
F (%)	—	—	—	—	NC	56.6[b] (4.5)	—	—
UE[c] (% of dose)	0.9 (0.4)	85.7 (12.5)	0.4 (0.2)	71.1 (8.0)	NT	NT	NT	NT

—, not applicable; CL_{total}, total plasma clearance; F, bioavailability; NC, not calculated; NT, not tested; t_{max}, time to reach maximum concentration; UE, urinary excretion; Vd_{ss}, volume of distribution at steady state.

[a]Plasma TP0473292 concentrations were below the lower limit of quantification (1 ng/ml) at all sampling time points.

[b]Bioavailability was calculated by dividing the dose-normalized $AUC_{0-\infty}$ of TP0178894 following oral administration of TP0473292 by the dose-normalized $AUC_{0-\infty}$ of TP0178894 following intravenous administration of TP0178894 shown in Table 3.

[c]Urinary excretion within 24 hours postdose was calculated by dividing excreted amount of the analyte compound (μmol) by the dose of TP0473292 (μmol).

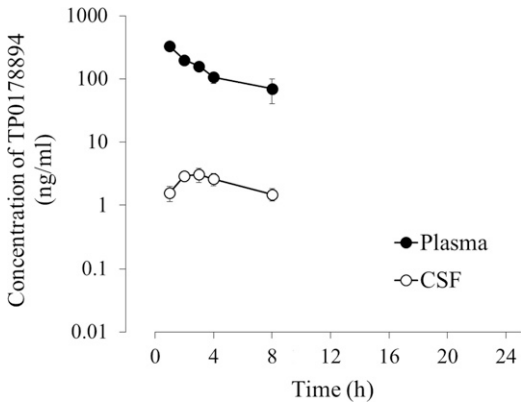

Fig. 6. Plasma and CSF concentration-time profiles of TP0178894 after a single oral administration of TP0473292 to nonfasted male SD rats at a dose of 1 mg/kg. Data are represented as the mean ± S.D. of three animals at each time point. The lower limit of quantification for TP0178894 was 0.1 ng/ml in plasma and 0.2 ng/ml in CSF.

be species dependent. Given the above, other prodrugs being unstable in the enterocytes also have the possibility to achieve good oral bioavailability as low permeable active compounds without active transport.

Since TP0178894 targets the central nervous system, we investigated the pharmacokinetics of TP0178894 in CSF at the effective dose of oral TP0473292 (1 mg/kg) using the rat forced-swimming test (Watanabe et al., 2022). Compared with the plasma pharmacokinetics, TP0178894 slowly penetrated and disappeared from the CSF, and the extent of CSF penetration was limited. As TP0178894 was not a P-glycoprotein substrate (data not shown), these pharmacokinetic profiles in CSF likely arise from the low membrane permeability of TP0178894 originated from its hydrophilicity, suggesting that similar results would be seen in humans.

Since no information was previously available, we evaluated the metabolism and disposition of ACA, the ester promoiety of TP0473292. In the metabolite profiling study of TP0473292 in hepatocytes, only acyl glucuronide, ACA-AG, was detected as a metabolite of ACA in all the species tested. In rats and monkeys, ACA-AG was excreted in urine with an excretion ratio comparable to that of TP0178894 after TP0473292 intravenous administration. These results suggested that ACA was rapidly metabolized and mainly excreted in urine as ACA-AG. Based on the in vitro metabolism of ACA in human hepatocytes, we expected that the metabolism and disposition of ACA in humans would be similar to that in the test animals. Although acyl glucuronides are known to be potentially associated with IDT risks because of their reactivity to macromolecules, the degradation $t_{1/2}$ of ACA-AG in the phosphate buffer (pH 7.4), which has been reported to be correlated with IDT risks (Sawamura et al., 2010), was much longer (79.2 hours) than the acyl glucuronides of diclofenac (1.23 hours) and ibuprofen (4.92 hours), which are classified in the "warning" category based on their IDT risks (Sawamura et al., 2010). This result indicates that ACA-AG had a high chemical stability and a low IDT risk, which was likely attributed to the bulky α carbon and a high steric hindrance of parent aglycone ACA that hinders the approach of nucleophiles and slows the intramolecular acyl migration process (Camilleri et al., 2018).

TABLE 6

Pharmacokinetic parameters of TP0178894 in plasma and CSF after a single oral administration of TP0473292 to nonfasted male SD rats at a dose of 1 mg/kg
Parameters were calculated from the mean concentration of three animals at each time point. The concentrations at 24 hours postdose were less than the lower limit of quantification (0.1 ng/ml in plasma and 0.2 ng/ml in CSF).

Parameter	Plasma	CSF
C_{max} (ng/ml)	321	2.78
t_{max} (h)	1.00	3.00
$t_{1/2}$ (h)	4.53	6.96[a]
AUC_{0-8h} (h·ng/ml)	999	14.9
CSF/plasma AUC_{0-8h} ratio (%)	—	1.49

—, not applicable; t_{max}, time to reach maximum concentration.
[a]The $t_{1/2}$ value was calculated based on the concentrations at the last two time points (4 and 8 hours postdose).

We also investigated the pharmacokinetic DDI potential of TP0473292 and its metabolites via P450 in humans. They showed no inhibitory potential on any of seven major P450 isoforms in either a reversible or a time-dependent manner and no induction potential on CYP1A2, CYP2B6, or CYP3A4. These results indicated that TP0473292 was unlikely to exert a pharmacokinetic DDI via P450 in humans.

In summary, the prodrug TP0473292 showed a faster conversion rate to its active metabolite than that of the successful oral prodrug MGS0274 in rat, monkey, and human tissue S9 fractions and showed complete conversion and good oral bioavailability as TP0178894 in the animals despite the presumably rapid conversion in the enterocytes. The ester promoiety, ACA, was rapidly metabolized to a chemically stable acyl glucuronide and excreted in urine in the animals, suggesting minimal safety concern. We concluded that TP0473292 would act as an ideal oral prodrug with a more complete conversion to its active metabolite than MGS0274 in humans. We have since confirmed our successful prodrug strategy in humans in subsequently conducted phase 1 clinical trials, where the prodrug TP0473292 (development code: TS-161) achieved good gastrointestinal absorption as TP0178894 (estimated bioavailability of over 85% under fed conditions), with very little plasma exposure to TP0473292 (approximately 0.1% of the C_{max} and AUC of TP0178894 in a molar concentration) (Watanabe et al., 2022). Additionally, the pharmacokinetics of TP0473292 and its metabolites in humans have been confirmed to be similar to those in the animals, as expected: TP0178894 distributed to CSF with slightly higher CSF-to-plasma AUC ratio (2.2%) to that in rats (1.5%) and eliminated from CSF slower than from plasma as observed in rats. The promoiety ACA was rapidly metabolized and mainly excreted in urine as ACA-AG (Watanabe et al., 2022).

This study indicated that the development of prodrugs with a high conversion rate in the enterocytes should not necessarily be avoided if the preclinical pharmacokinetics are carefully evaluated. Furthermore, we showed that ACA has potential to be a useful ester promoiety for a hydrophilic active compound by giving appropriate lipophilicity to enhance membrane permeability, undergoing rapid hydrolysis by CES(s), and disappearing without DDI or safety concern after liberating.

Authorship Contributions

Participated in research design: Inatani, Ochi, Kinoshita, Yamaguchi, Endo.

Conducted experiments: Inatani, Ochi.

Performed data analysis: Inatani, Ochi, Kinoshita, Yamaguchi, Endo.

Wrote or contributed to the writing of the manuscript: Inatani, Ochi, Kinoshita, Yamaguchi, Endo.

References

Aboul-Fadl T, Sheha MM, El-Azab AS, and Abdel-Aziz HA (2011) Amantadine amides prodrugs as hepatic delivery systems to enhance its activity against HCV. *Dig J Nanomater Biostruct* **6**:1675–1683.

Beaumont K, Webster R, Gardner I, and Dack K (2003) Design of ester prodrugs to enhance oral absorption of poorly permeable compounds: challenges to the discovery scientist. *Curr Drug Metab* **4**:461–485.

Boudinot FD and Jusko WJ (1984) Fluid shifts and other factors affecting plasma protein binding of prednisolone by equilibrium dialysis. *J Pharm Sci* **73**:774–780.

Camilleri P, Buch A, Soldo B, and Hutt AJ (2018) The influence of physicochemical properties on the reactivity and stability of acyl glucuronides †. *Xenobiotica* **48**:958–972.
Chaki S (2017) mGlu2/3 receptor antagonists as novel antidepressants. *Trends Pharmacol Sci* **38**:569–580.
Chaki S and Fukumoto K (2019) Role of serotonergic system in the antidepressant actions of mGlu2/3 receptor antagonists: similarity to ketamine. *Int J Mol Sci* **20**:1270.
Di L (2019) The impact of carboxylesterases in drug metabolism and pharmacokinetics. *Curr Drug Metab* **20**:91–102.
Fujiyama N, Miura M, Satoh S, Inoue K, Kagaya H, Saito M, Habuchi T, and Suzuki T (2009) Influence of carboxylesterase 2 genetic polymorphisms on mycophenolic acid pharmacokinetics in Japanese renal transplant recipients. *Xenobiotica* **39**:407–414.
Gadient RA, Wedel P, Frisbie V, Leuchter AF, Targum SD, Truong C, and Hutchinson JH (2012) Safety, pharmacokinetic and pharmacodynamic profile of BCI-632, a selective metabotropic glutamate 2/3 receptor antagonist, in healthy human subjects. Paper presented as: Abstract of *Annual Meeting of Society for Neuroscience*; Oct 2012; New Orleans, LA. Abstract 841.20.
González-Méndez I, Solano JD, Porcu P, Ruiu A, Rojas-Aguirre Y, and Rivera E (2019) Optimized synthesis, characterization and in vitro systematic evaluation of adamantane-doxorubicin prodrugs sensitive to pH in breast cancer cells. *J Mol Struct* **1177**:143–151.
Haux JE, Lockridge O, and Casida JE (2002) Specificity of ethephon as a butyrylcholinesterase inhibitor and phosphorylating agent. *Chem Res Toxicol* **15**:1527–1533.
Jinno N, Ohashi S, Tagashira M, Kohira T, and Yamada S (2013) A simple method to evaluate reactivity of acylglucuronides optimized for early stage drug discovery. *Biol Pharm Bull* **36**:1509–1513.
Kinoshita K, Ochi M, Iwata K, Fukasawa M, and Yamaguchi JI (2019) Preclinical disposition of MGS0274 besylate, a prodrug of a potent group II metabotropic glutamate receptor agonist MGS0008 for the treatment of schizophrenia. *Pharmacol Res Perspect* **7**:e00520.
Masaki K, Taketani M, and Imai T (2006) First-pass hydrolysis of a propranolol ester derivative in rat small intestine. *Drug Metab Dispos* **34**:398–404.
Monrad RN, Errey JC, Barry CS, Iqbal M, Meng X, Iddon L, Perrie JA, Harding JR, Wilson ID, Stachulski AV, et al. (2014) Dissecting the reaction of Phase II metabolites of ibuprofen and other NSAIDS with human plasma protein. *Chem Sci (Camb)* **5**:3789–3794.
Nakamura M, Kawakita Y, Yasuhara A, Fukasawa Y, Yoshida K, Sakagami K, and Nakazato A (2006) In vitro and in vivo evaluation of the metabolism and bioavailability of ester prodrugs of mgs0039 (3-(3,4-dichlorobenzyloxy)-2-amino-6-fluorobicyclo[3.1.0]hexane-2,6-dicarboxylic Acid), a potent metabotropic glutamate receptor antagonist. *Drug Metab Dispos* **34**:369–374.
Nakazato A, Sakagami K, Yasuhara A, Ohta H, Yoshikawa R, Itoh M, Nakamura M, and Chaki S (2004) Synthesis, in vitro pharmacology, structure-activity relationships, and pharmacokinetics of 3-alkoxy-2-amino-6-fluorobicyclo[3.1.0]hexane-2,6-dicarboxylic acid derivatives as potent and selective group II metabotropic glutamate receptor antagonists. *J Med Chem* **47**:4570–4587.
Ochi M, Kinoshita K, Yamaguchi JI, and Endo H (2022) Bottom-up physiologically based pharmacokinetic modelling for predicting the human pharmacokinetic profiles of the ester prodrug MGS0274 and its active metabolite MGS0008, a metabotropic glutamate 2/3 receptor agonist. *Xenobiotica* **52**:119–128.
Otake N, Hashihayata T, Matsuda Y, Masuda S, and Yamauchi Y (2017) inventors, Taisho Pharmaceutical Co., Ltd., assignee. Prodrug of amino acid derivative. Patent WO2017/183734. 2017 Oct 26.
Sawamura R, Okudaira N, Watanabe K, Murai T, Kobayashi Y, Tachibana M, Ohnuki T, Masuda K, Honma H, Kurihara A, et al. (2010) Predictability of idiosyncratic drug toxicity risk for carboxylic acid-containing drugs based on the chemical stability of acyl glucuronide. *Drug Metab Dispos* **38**:1857–1864.
Shimizu M, Fukami T, Nakajima M, and Yokoi T (2014) Screening of specific inhibitors for human carboxylesterases or arylacetamide deacetylase. *Drug Metab Dispos* **42**:1103–1109.
Tachibana S, Fujimaki Y, Yokoyama H, Okazaki O, and Sudo K (2005) In vitro metabolism of the calmodulin antagonist DY-9760e (3-[2-[4-(3-chloro-2-methylphenyl)-1-piperazinyl]ethyl]-5,6-dimethoxy-1-(4-imidazolylmethyl)-1H-indazole dihydrochloride 3.5 hydrate) by human liver microsomes: involvement of cytochromes p450 in atypical kinetics and potential drug interactions. *Drug Metab Dispos* **33**:1628–1636.
Takahashi M, Washio T, Suzuki N, Igeta K, and Yamashita S (2010) Investigation of the intestinal permeability and first-pass metabolism of drugs in cynomolgus monkeys using single-pass intestinal perfusion. *Biol Pharm Bull* **33**:111–116.
Takano H, Yamaguchi JI, Kato S, Hamada M, Tada M, and Endo H (2021) Downregulation of CYP1A2, CYP2B6, and CYP3A4 in human hepatocytes by prolyl hydroxylase domain 2 inhibitors via hypoxia-inducible factor-α stabilization. *Drug Metab Dispos* **49**:20–30.
Trapa PE, Beaumont K, Atkinson K, Eng H, King-Ahmad A, Scott DO, Maurer TS, and Di L (2017) In vitro-in vivo extrapolation of intestinal availability for carboxylesterase substrates using portal vein-cannulated monkey. *J Pharm Sci* **106**:898–905.
Umehara K, Zollinger M, Kigondu E, Witschi M, Juif C, Huth F, Schiller H, Chibale K, and Camenisch G (2016) Esterase phenotyping in human liver in vitro: specificity of carboxylesterase inhibitors. *Xenobiotica* **46**:862–867.
Urabe H, Miyakoshi N, Ohtake N, Nozoe A, Ochi M, Fukasawa M, Kinoshita K, Yamaguchi JI, Marumo T, Hikichi H, et al. (2020) Discovery of MGS0274, an ester prodrug of a metabotropic glutamate receptor 2/3 agonist with improved oral bioavailability. *Eur J Med Chem* **203**:112521.
Wadkins RM, Hyatt JL, Wei X, Yoon KJP, Wierdl M, Edwards CC, Morton CL, Obenauer JC, Damodaran K, Beroza P, et al. (2005) Identification and characterization of novel benzil (diphenylethane-1,2-dione) analogues as inhibitors of mammalian carboxylesterases. *J Med Chem* **48**:2906–2915.
Wanka L, Iqbal K, and Schreiner PR (2013) The lipophilic bullet hits the targets: medicinal chemistry of adamantane derivatives. *Chem Rev* **113**:3516–3604.
Watanabe A, Fukami T, Nakajima M, Takamiya M, Aoki Y, and Yokoi T (2009) Human arylacetamide deacetylase is a principal enzyme in flutamide hydrolysis. *Drug Metab Dispos* **37**:1513–1520.
Watanabe M, Marcy B, Hiroki A, Watase H, Kinoshita K, Iijima M, Marumo T, Zarate Jr CA, and Chaki S (2022) Evaluation of the safety, tolerability, and pharmacokinetic profiles of TP0473292 (TS-161), a prodrug of a novel orthosteric mGlu2/3 receptor antagonist TP0178894, in healthy subjects and its antidepressant-like effects in rodents. *Int J Neuropsychopharmacol* **25**:106–117.
Watanabe M, Marcy B, Kinoshita K, Fukasawa M, Hikichi H, Chaki S, Okuyama S, Gevorkyan H, and Yoshida S (2020) Safety and pharmacokinetic profiles of MGS0274 besylate (TS-134), a novel metabotropic glutamate 2/3 receptor agonist prodrug, in healthy subjects. *Br J Clin Pharmacol* **86**:2286–2301.
Witkin JM (2020) mGlu2/3 receptor antagonism: A mechanism to induce rapid antidepressant effects without ketamine-associated side-effects. *Pharmacol Biochem Behav* **190**:172854.

Address correspondence to: Shoko Inatani, Drug Metabolism and Pharmacokinetics, Drug Safety and Pharmacokinetics Laboratories, Research Headquarters, Taisho Pharmaceutical Co., Ltd., 1-403, Yoshino-cho, Kita-ku, Saitama-shi, Saitama 331-9530, Japan. E-mail: s-inatani@taisho.co.jp